LHC APERTURE AND COMMISSIONING OF THE COLLIMATION SYSTEM

S. Redaelli*, R. Aßmann, G. Robert-Demolaize, CERN, Geneva, Switzerland

Abstract

The design LHC aperture and its dependence on various optics imperfections are discussed. The cleaning performance of the LHC collimation system is reviewed. The loss maps around the LHC ring at injection and collision energy are compared with the quench limit of superconducting magnets. The effect of optics imperfections is also discussed. These studies are based on the results of tracking simulations of the beam halo and on a detailed aperture model of the full LHC ring, with spatial resolution of 10 cm over the total length of 27 km. Experimental results from the collimator test with beam at the SPS are reviewed and specific issues related to the commissioning of the collimation system, such as alignment of the jaw with respect to the beam envelope and adjustment of the jaw angle, are discussed.

INTRODUCTION

The beam halo cleaning is the primary purpose of the LHC collimation system. During LHC operation, proton losses must be kept under control in order to avoid quenches of the superconducting magnets. The available information [1] on quenches induced by proton losses suggests that at the LHC the maximum allowed loss rate of protons are [2]:

$$R_q^{\text{inj}} = 7.0 \times 10^8 \text{ protons/m/s } (450 \text{ GeV}) \quad (1)$$

$$R_q^{\text{low}\beta} = 7.6 \times 10^6 \text{ protons/m/s } (7 \text{ TeV}) \quad (2)$$

For a nominal beam intensity of 3×10^{14} protons, losses must then be controlled to within $10^{-6} - 10^{-9}$ of the total beam population. Failing to control beam losses will impose limitations to the maximum beam intensity. Therefore, understanding the ring aperture and the loss locations is crucial for the LHC commission. The simplified linear models available until recently were used to design LHC aperture but could not take into account the dynamics of the *secondary* and *tertiary* beam halos, i.e. the beam protons that escape from the primary and secondary collimators, respectively. The halo particles that escape from the cleaning insertion may experience large betatron kicks and energy errors due to the scattering in the collimator jaws and can in principle be lost anywhere in the machine. A detailed tracking with a correct treatment of chromatic effects and non-linear fields is required to properly simulate the dynamics of this particles. An aperture model of the

---

*Stefano.Redaelli@cern.ch

Table 1: Tolerances taken into account in the design of the LHC aperture [3].

Tolerance	Design value
Manufacturing	$\leqq 1.6$ mm
Alignment	$\leqq 1.6$ mm
Separation/crossing schemes	$\leqq 1.5$ mm
Spurious dispersion	27 % of arc (normal.)
Allowance for $\Delta p/p$	0.05%
Closed orbit (radial), injection	4.0 mm
Closed orbit (radial), 7 TeV	3.0 mm
Beta-beat ($\Delta\beta/\beta$)	21 %

full ring is required to understand at which locations protons can be lost. New simulations tools have been set-up to predict the proton loss locations all around the ring with spatial resolution of 10 cm [4]. This advances considerably the state-of-the-art of loss pattern studies. The outcome of these loss simulations are discussed in view of the commissioning of the LHC collimation system.

In this paper, LHC aperture is briefly reviewed and the aperture bottlenecks at injection and at 7 TeV are identified. Then, loss pattern around the ring are compared with the quench limits for a perfect machine and for machines with some optical imperfections. In addition, the highlights of the collimation measurements with beam at the SPS are reviewed, with particular emphasis to the topics that have direct implications on the commissioning of the collimator system at the LHC.

REVIEW OF THE LHC APERTURE

Aperture for the LHC optics V6.5

The LHC aperture was designed with the APL code [3], which uses a simplified linear model to calculate the envelope of the secondary beam halo all around the LHC ring. The mechanical and optical tolerances listed in Table 1 were taken into account. The LHC aperture was then designed following the criterion that anywhere in the machine the secondary beam halo should just touch the inner wall of the cold apertures. It has been demonstrated [5] that this corresponds to ensuring a radial geometrical acceptance of $9.8\,\sigma$, or, correspondingly, a vertical and horizontal acceptance of $8.5\,\sigma$. Here, $\sigma = \sqrt{\beta\epsilon}$ is the local beam size calculated from beta functions and the emittance. The design criterion implicitly assumes that the population of the tertiary beam halo is below the quench limit of super-
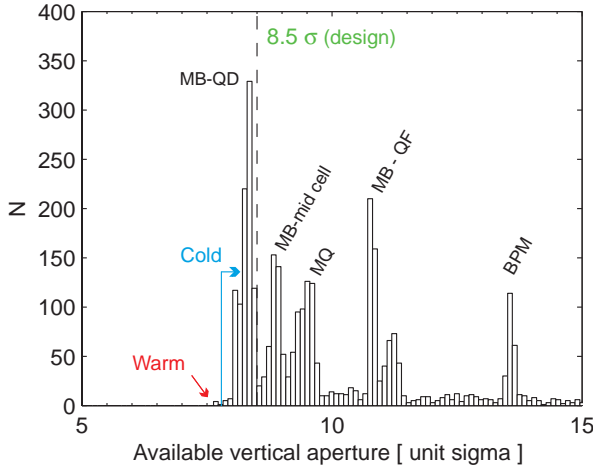
Figure 1: Distribution of vertical available mechanical aperture for the full LHC ring at injection (450 GeV). Aperture is given in σ units. The peak below the design value of $8.5\,\sigma$ corresponds to the arc dipole close to the horizontally defocussing quadrupoles (MB-QD), where the vertical beam size is larger. Elements below $7.8\,\sigma$ are operated at warm temperature.

Table 2: Minimal horizontal and vertical apertures at injection (450 GeV) and at top energy (7 TeV, with $\beta^* = 0.55$ m) for warm and cold elements.

	450 GeV		7 TeV	
	Warm	Cold	Warm	Cold
Beam 1				
Horizontal	6.78	7.88	28.1	8.90
Vertical	7.68	7.79	8.34	8.43
Beam 2				
Horizontal	6.68	7.70	27.6	8.13
Vertical	7.65	7.60	8.69	8.75

conducting magnets. The studies did not include detailed tracking of large amplitude and off-momentum halo particles.

Here, we review the aperture of the LHC optics version 6.5. A modified version of the APL, which allows calculating the available horizontal and vertical mechanical apertures at each lattice component, was used. For example, the distribution of available vertical aperture at injection (450 GeV) is shown in Fig. 1. At 450 GeV, the aperture is limited by the arcs. Aperture bottlenecks are distributed all around the ring and this results in a large number of superconducting magnets (main dipoles, MB's, and main quadrupoles, MQ's) which might in principle be hit by the secondary beam halo. Figure 1 shows that many magnets are below the target values of $8.5\,\sigma$ (dashed lines in the graphs). The minimum aperture for cold elements is $7.60\,\sigma$. In Table 2 the various aperture bottleneck of warm and cold elements are shown, also for the 7 TeV case.

At 7 TeV, the arc aperture is no longer critical because the betatron amplitudes are approximately 4 times smaller than at 450 GeV due to the acceleration damping. On the other hand, for squeezed optics ($\beta^* = 0.55$ m), the aperture is limited by the superconducting triplets, where beta-functions as large as ≈ 4500 m are required to achieve small beam sizes at the interaction points (high luminosity experimental are located at IP1 and IP5). In addition, the available aperture is further reduced by the beam offsets due to the separation and crossing schemes. The aperture bottleneck at the triplets is $8.1\,\sigma$, i.e. approximately $0.5\,\sigma$ smaller than the design value. It should be noted that, unlike for the injection case, only a few magnets are below the design value.

Dependence on energy spread, beta-beat and closed orbit

In the aperture design, a margin $\Delta p/p = 0.05\,\%$, on top of the bucket width, has been accounted for as allowance for energy sweeps for chromaticity measurements. One can reasonably assume that no chromaticity measurements should be carried out immediately after the beam injection in case that large beam oscillations take place. It has been verified that without taking into account the $0.05\,\%$ budget of $\delta p/p$ one would typically gain $0.6\,\sigma$ on the horizontal aperture bottleneck at injection.

Otherwise, the only operational parameters available for optimizing the aperture are the beta-beat and the closed orbit. The other parameters of Table 1 are fixed by the mechanical and alignment tolerances and by the expected field errors in the LHC magnets. One can illustrate the interplay of beta-beat and closed orbit by writing the total aperture margin allocated for the two combined effects, ΔA, as

$$\Delta A = n_c \Delta \sigma^{\beta - \text{beat}} + \Delta^{\text{CO}}. \qquad (3)$$

The first term of Eq. (3) right-hand-side, $n_c \Delta \sigma^{\beta - \text{beat}}$, is the beam size variation due to the local variation of the beta function, $\Delta\beta/\beta$, weighted with the number of sigma $n_c = 8.5$ (design value). The second term (Δ^{CO}) represents the local closed-orbit error. The maximum allowed beta-beat error as a function of the local closed orbit error:

$$\left(\frac{\Delta\beta}{\beta_0}\right)_{\text{allowed}} = \left[\frac{\Delta A - \Delta^{\text{CO}}}{n_c} + \sigma_0\right]^2 \frac{1}{\sigma_0^2} - 1, \qquad (4)$$

where $\sigma_0 = \sqrt{\beta_0 \epsilon}$ is the unperturbed beam size. The contribution from the dispersion is disregarded because it is taken into account separately from the betatron contribution. For example, the allowed beta-beat in the arcs at injection is shown in Fig. 2. The total budget $\Delta A = 5$ mm is assumed. It is noticed that, by design, there is basically no margin to optimize the aperture in the arcs. The $20\,\%$ allocated budget for beta-beat is barely compatible with the assumed maximum closed orbit offset of 4 mm. For the 7 TeV case, it is found that the closed orbit tolerance of
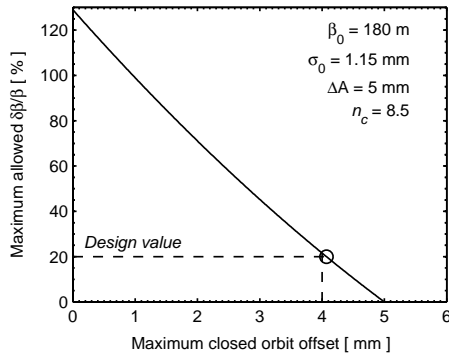
Figure 2: Maximum allowed beta-beat as a function of the closed orbit error, as calculated in Eq. (4). The case of LHC arcs at $450\,\mathrm{GeV}$ is considered. The design values $\Delta\beta/\beta = 20\,\%$ and $\Delta^{\mathrm{CO}} = 4\,\mathrm{mm}$ are also shown (dashed lines).

$3\,\mathrm{mm}$ at the triplets allows for a maximum beta-beat error up to approximately $30\,\%$.

CLEANING PERFORMANCE AND LOSS MAPS

The linear model based on the periodic Twiss functions around the ring is very useful to design the aperture but is not suitable for detailed studies of beam losses. A tracking of halo particles, which must treat properly the large betatron amplitudes and energy errors of the halo particles at the exit of the cleaning insertion, is instead required.

Tools for halo tracking and loss maps

The generation of secondary and tertiary beam halos in the two-stage collimation system and the multi-turn tracking of halo particles are performed with a program [4] that combines the collimator scattering routine K2 [7] with the tracking program SixTrack [8]. SixTrack performs a thin-lens tracking takes into account the chromatic correction of off-momentum particles and higher order non-linear errors. This tool is used to calculate the cleaning inefficiency of the two-stage collimation system (see next section) and to save the particle trajectories for an offline analysis of beam losses.

Loss maps are produced with an independent program that takes as input the multi-turn trajectories of halo particles and looks for the ring locations where they hit the aperture inner wall. This is done as illustrated in Fig. 3. From the thin-lens tracking, the particle coordinates are saved at each magnetic element that can bend the particle trajectory (typical distance between consecutive elements $\leq 100\,\mathrm{m}$). This provides the multi-turn trajectories of the halo particles. The aperture program looks for the first element where the particle is lost and then traces back the particle position until it localizes the loss point with a resolution of $10\,\mathrm{cm}$. This procedure relies on interpolating of the aperture along the full ring and is effectively equivalent to checking the transverse positions of each particle in 270000 points. The aperture program features a 2-
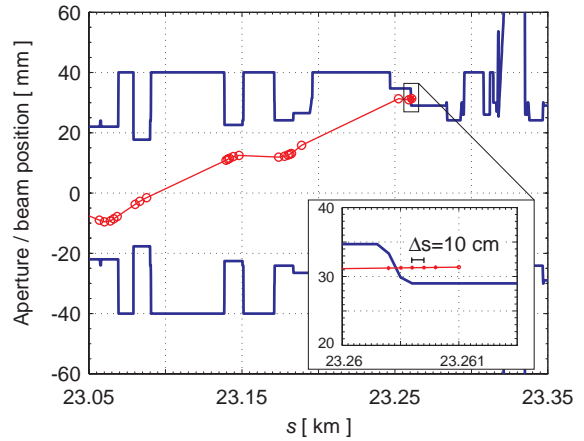

Figure 3: Example of a halo particle (red line) that hits the LHC aperture (blue line).

dimensional treatment of the various LHC aperture types.

In the simulations presented here, the gaps of primary and secondary collimators are set to $6\,\sigma$ and $7\,\sigma$, respectively, and are centred around the local closed orbit (unless otherwise specified). Beam halos are generated from a multi-turn tracking of initial particle distributions which then interact with the primary collimators. The initial horizontal distribution in normalized phase space is an annulus with radii $R_x = \sqrt{\hat{X}^2 + \hat{X}'^2} = 6.003$ and $R_y = \sqrt{\hat{Y}^2 + \hat{Y}'^2} = 0$ and thickness $\delta\sigma = 0.0015\,\sigma$ (flat distributions). This is chosen to obtain the correct impact parameters on the primary collimators, according to the diffusion speed calculated in [9]. This produces the so-called *horizontal* beam halo. Similarly, for the *vertical* halo we take $A_x = 0$ and $A_y = 6.003\,\sigma$. An example of input distribution is shown in Fig. 4. Typically, distributions of 5×10^6 particles per halo type are tracked for 200 turns.

Cleaning inefficiency for a perfect machine

The *cleaning inefficiency* $\eta_c(A_0)$ of the collimation system is defined [2] as a function of the particle amplitude A_0 as the number of beam protons with aperture above A_0,
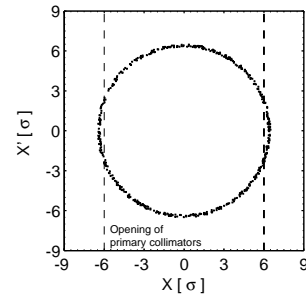

Figure 4: Example of input distribution generated with the parameters $R_x = 6.4\,\sigma$ and $\delta\sigma = 0.2\sigma$. In the simulations, $R_x = 6.003\,\sigma$ and $\delta\sigma = 0.0015\,\sigma$ are used. The opening of primary collimators is $6\,\sigma$ (dashed lines).
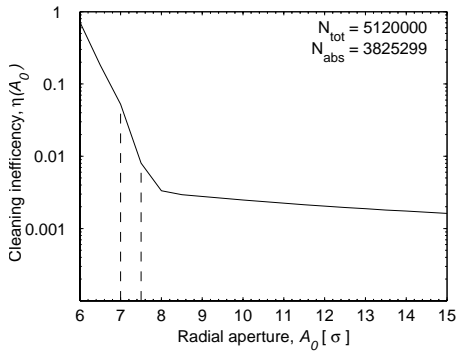
Figure 5: Cleaning inefficiency, $\eta_c(A_0)$, as a function of the radial aperture, A_0, as defined in Eq. (5). The case of a vertical halo at injection (450 GeV) is considered.

Figure 6: Cleaning inefficiency, $\eta_c(A_0)$, as a function of the radial aperture, A_0, as defined in Eq. (5). The case of a vertical halo at 7 TeV with squeezed optics at IP1 and IP5.

$N_p(A > A_0)$, divided by the total number of absorbed protons in the cleaning insertion, N_{abs}:

$$\eta_c(A_0) = \frac{N_p(A > A_0)}{N_{\text{abs}}}. \tag{5}$$

This expression has the advantage of providing a definition of the halo population independent of the longitudinal coordinate s. One can also define a *local cleaning inefficiency*, $\tilde{\eta}_c$, by normalizing η_c by the dilution length of particle losses, L_{dil}:

$$\tilde{\eta}_c = \frac{\eta_c}{L_{\text{dil}}}, \tag{6}$$

where the explicit dependence on A_0 has been dropped. Typically, the value $L_{\text{dil}} = 50$ m is assumed [1]. The concept of local cleaning inefficiency will be useful later for comparing the proton losses with the quench limit of superconducting magnets.

In Figures 5 and 6, two examples of cleaning inefficiency at 450 GeV and at 7 TeV are shown. These curves have been obtained by tracking $\approx 5 \times 10^6$ protons for 200 turns. A typical value of η_c at injection for the minimum aperture $A = 7.5\sigma$ of the cold elements (see Section) is 8×10^{-3}. It is interesting to note that, if somewhere in the machine an aperture bottleneck exist at $A = 7.0\,\sigma$, i.e. $0.5\,\sigma$ below the nominal value, the local losses there can increase by more than a factor 6. This suggest that a control of the aperture all around the ring is highly recommended before starting high intensity runs. The cleaning inefficiency at 7 TeV is shown in Fig. 6. As a design feature, the LHC collimation system provides a better cleaning performance at 7 TeV than at injection energy. At an aperture of 10σ, the cleaning inefficiencies are typically below 10^{-3}.

Definition of quench limits

Before discussing in details the loss maps around the LHC ring, it is worth briefly reviewing the assumed definitions of quench limits for the superconducting magnets. So far, the results of [1] have been used as reference. More details, which include latest estimates of quench limits for various magnet types other than the LHC main dipoles, are
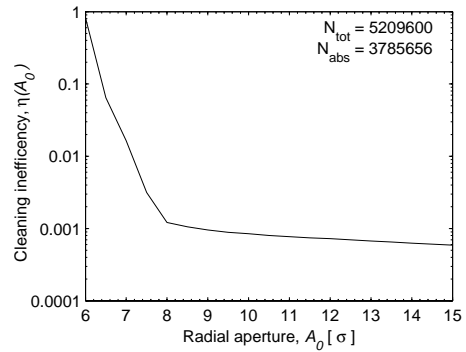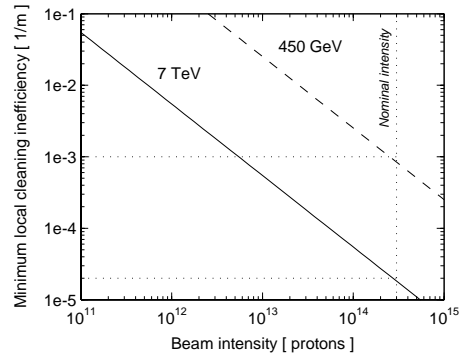

Figure 7: Minimum required cleaning inefficiency versus total beam intensity as required at 450 GeV (dashed line) and at 7 TeV (solid line) to keep proton beam losses below the quench limit.

discussed in these proceedings [11]. One can define a critical local inefficiency at the quench limit, $\tilde{\eta}_c^q$, as

$$\tilde{\eta}_c^q = \frac{\eta_c^q}{L_{\text{dil}}} = \frac{\tau R_q}{N_{\text{tot}}}, \tag{7}$$

where τ is the beam lifetime and N_{tot} is the total beam intensity (see also [2]). For an assumed value of expected minimum beam lifetime, Eq. (7) can then be used to estimate the minimum allowed local cleaning inefficiency which must be achieved in order to stay below the quench limit of superconducting magnets. In Figure 7, $\tilde{\eta}_c^q$ is plotted as a function of the beam intensity for the LHC beam at 450 GeV (dashed line) and at 7 TeV (solid line). Beam lifetimes of $\tau^{\text{inj}} = 0.1$ h and $\tau^{\text{low}\beta} = 0.2$ h are assumed for injection and top energy, respectively [2]. The quench limits of Eqs. (1) and (2) are assumed. For the nominal beam intensity of $N_{\text{tot}} = 3 \times 10^{14}$ protons, the following values are calculated:

$$\begin{aligned}
\tilde{\eta}_c^{q,\text{inj}} &\approx 1 \times 10^{-3} \quad (450\,\text{GeV}), \\
\tilde{\eta}_c^{q,\text{low}\beta} &\approx 2 \times 10^{-5} \quad (7\,\text{TeV}),
\end{aligned} \tag{8}$$

which from now on will be regarded as the reference quench limits to be compared with the achieved local cleaning inefficiency at the superconducting magnets. Since no
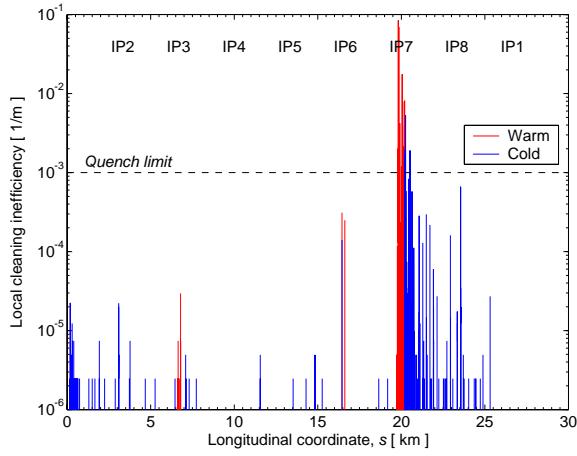
271

Figure 8: Local cleaning inefficiency at injection (450 GeV), calculated as in Eq. (9), versus longitudinal coordinate for an *horizontal halo*. Red and blue peaks correspond to losses in warm and cold regions, respectively. 5.1×10^6 particles are tracked.
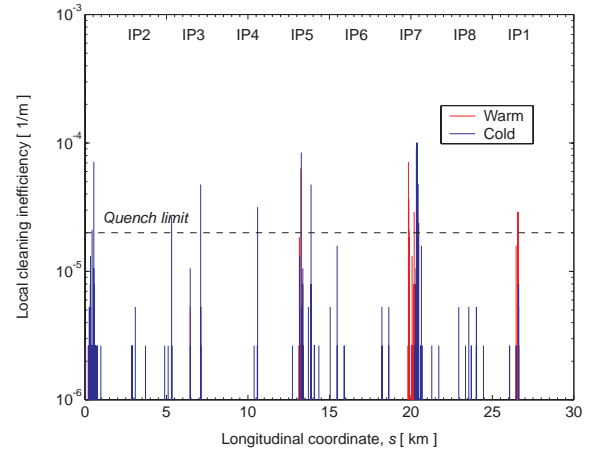

Figure 9: Local cleaning inefficiency at 7 TeV, calculated as in Eq. (9), versus longitudinal coordinate for a *vertical halo*. Red and blue peaks correspond to losses in warm and cold regions, respectively. 5.1×10^6 particles are tracked.

information has been available so far for other magnets than the LHC main dipoles, the quench limits of Eqs. (8) are assumed to apply to all LHC cold elements.

Loss maps around the ring for a perfect machine

The comparison with the quench limits of Eq. (8) is carried out by computing the achieved local cleaning inefficiency from the loss maps around the ring. This is done by calculating

$$\tilde{\eta}_c(s) = \frac{1}{\Delta s} \frac{N_{\text{loss}}(s \to s + \Delta s)}{N_{\text{abs}}}, \qquad (9)$$

where N_{abs} is the total number of absorbed particles in the cleaning insertion and $N_{\text{loss}}(s \to s + \Delta s)$ is the number of particles lost at the s location, in the bin of size $\Delta s = 10 \, \text{cm}$ (resolution of the aperture model). The function $\tilde{\eta}_c(s)$ of Eq. (9) is shown in Figs. 8 and 9 for the 450 GeV and 7 TeV cases, respectively. A perfect machine, with no optics nor alignment errors, is considered. The 7 TeV case is obtained with squeezed optics at IP1 and IP5 ($\beta^* = 0.55 \, \text{m}$) and with injection optics at IP2 and IP8 ($\beta^* = 10 \, \text{m}$). Red and blue lines correspond to warm and cold elements, respectively.

Even for a perfect machine, it is noticed that at several locations the losses are above, or close to, the quench limit, both at injection and at top energy. At injection, the largest loss at cold elements are located in the arc 7-8, just downstream of the betatron cleaning insertion (IR7). Additional particle absorbers, which are not yet included in the present aperture model, are being designed to protect the dispersion suppressor downstream of the cleaning insertion. They are expected to significantly reduce the peak losses at the most critical elements. Nevertheless, losses are also found at unexpected locations such as some trim quadrupoles in the

IR6 insertion, for which no local protecting has been foreseen.

At 7 TeV, the performance of the collimation system is better and $\tilde{\eta}_c$ is typically below 10^{-4}. However, the quench limit is 50 times smaller than at 450 GeV and many more locations are above the quench threshold of Eq. (8). Notably, several peaks are found at IP8 even if the optics is not squeezed (at the triplets, $\beta \leq 350 \, \text{m}$). The implications of this unexpected losses shall be understood. Below, some examples are further discussed.

As an example, Fig. 10 shows the longitudinal (top graph) and transverse (bottom graph) distribution of losses at the superconducting triplet upstream of IP1 (vertical crossing), as simulated at 7 TeV with squeezed optics ($\beta^* = 0.55 \, \text{m}$). Longitudinally, the proton losses follow the path of the beta function, which reach the value of $\approx 4500 \, \text{m}$ at the quadrupole MQXB.B2L1. Transversally, the losses are concentrated on the horizontal walls of the beam screen. Dedicated tertiary collimators [10], which have not been included in the model yet, will intercept these protons before they hit the superconducting quadrupole. On the other hand, it is found that at IP5 (horizontal crossing), also skew losses arise. This is shown in Fig. 11. No skew tertiary collimator have been foreseen in this region. It remain to be verified whether the available horizontal and vertical collimators could be closed to gaps small enough to intercept the skew protons.

As a last example, Fig. 12 shows the transverse distribution of losses along 45 m in the dispersion suppressor downstream of IR7. At injection (left graph), both horizontal and vertical losses are found whereas at 7 TeV (right graph) the losses are mainly concentrated on the aperture inner wall ($x < 0$). The reason for this difference is that at 450 GeV the motion of the halo particles is strongly affected by the large betatron oscillations. On the other hand, at 7 TeV the adiabatic energy damping reduces the contri-
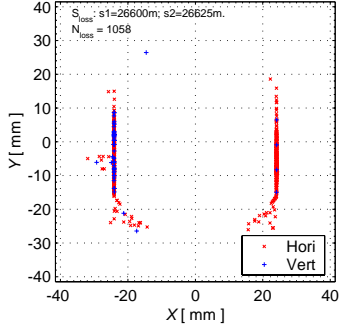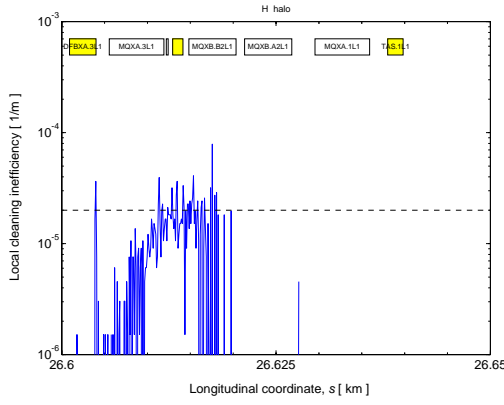
Figure 10: Longitudinal (top graph) and transverse (bottom graph) distribution of losses at the triplet upstream of IP1, as simulated at 7 TeV with squeezed optics ($\beta^* = 0.55$ m).
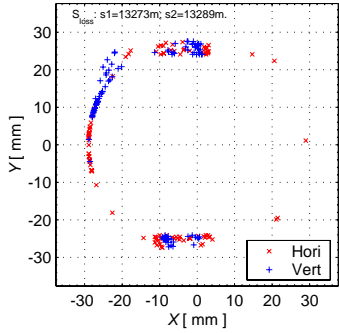

Figure 11: Scatter plot of the transverse loss distribution at the triplet of upstream of IP5, as simulated at 7 TeV with squeezed optics ($\beta^* = 0.55$ m).

bution of the betatron motion. For increasing beam energy, E_b, the betatron oscillations decrease as $E_b^{-0.5}$. For the LHC, the beam size at top energy is ≈ 4 times smaller than at injection. As a result of this, the losses at 7 TeV are driven by energy error effects. This example illustrates that the location of beam loss monitors and the understanding of quench limit depends on the optics under consideration.

Effect of optical imperfections

The results discussed so far were obtained for a perfect machine. The full analysis of effects on cleaning ineffi-
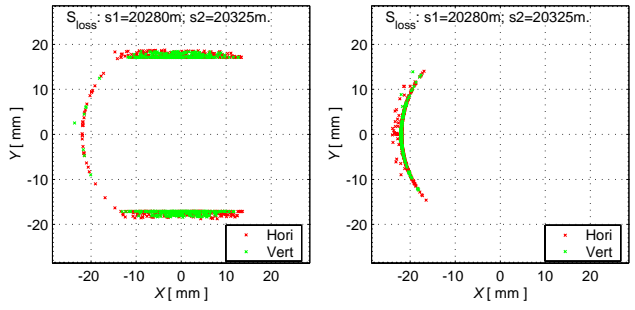

Figure 12: Transverse distribution of losses along 45 m of the dispersion suppressor downstream of IR7, as simulated at 450 GeV (left graph) and at 7 TeV (right graph). Both horizontal and vertical halo are considered.
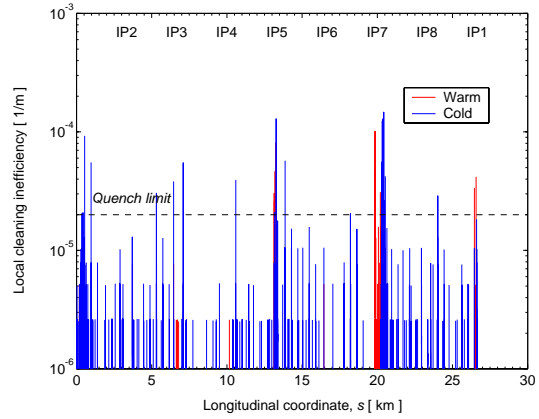

Figure 13: Maximum local cleaning inefficiency obtained for the 7 TeV case with 10 seeds for closed orbit errors.

ciency and loss maps from magnetic and alignment errors, remains to be carried out. Here, we concentrate on the effect of closed orbit and beta-beat.

To simulate the effect of closed orbit errors, ten different orbits were generated with MADX [6] by horizontally and vertically misaligning the lattice main quadrupoles. The obtained orbits have a typical RMS error of 1 mm and peak values of 3-4 mm. They are added off-line to the particle trajectories before running the aperture program. In Figure 13, the maximum cleaning inefficiency obtained for the 10 closed orbit seeds is shown for the 7 TeV case. It is found that local losses can be easily increased by a factor 10 if the closed orbit errors are taken into account. Several cold locations are now 10 times above the assumed quench limits. A similar increase of losses is observed for the injection case. These results are still obtained with a perfect adjustment of the collimators (nominal jaw centring and depth). An additional degradation of the cleaning performance by a factor ≈ 2 is expected for a imperfect system.

Although the closed orbit errors dominate the aperture (see Fig. 2), beta-beat errors have also an impact on the cleaning performance. Figure 14 shows the cleaning efficiency at $8, 10$ and $12\,\sigma$ as a function of a *static* beta-beat
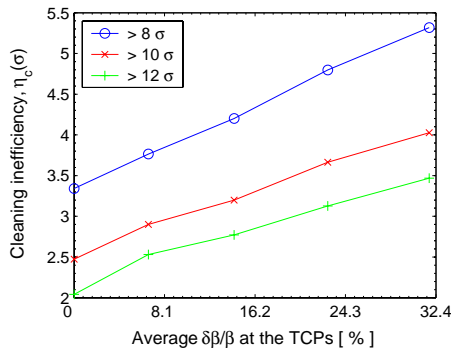
Figure 14: Degradation of cleaning inefficiency for a static beta-beat error. The collimators are set to the nominal depths that matches the local beam size.

error. Here, it is assumed that a beta-beat is induced by some quadrupole field errors and that the IR7 collimators are then adjusted with their nominal depths to the match the local beam size. A reduction of the cleaning performance is then induced by beta-beat induced errors of the phase advances in the cleaning insertion. It is found that for some phases of the beta-beat, the cleaning inefficiency can be increased by up to 30 % for $\Delta\beta/\beta \approx 20\,\%$. In addition, depending on the amplitude of the beat, beam losses can locally be increased above the quench limits.

TESTS WITH BEAM AT THE SPS

Experimental setup

Collimator tests with beams were carried out in October 2004 at the SPS. A prototype of horizontal collimator, with all the mechanical functionalities required by the LHC phase I collimation (carbon jaws) [10], was installed in the SPS and tested with different beam types. Table 3 summarizes the beam parameters for the various cases (low and high intensity runs). The main goal of the tests with beam was to demonstrate the required functionalities of the LHC collimator design, such as mechanical movements, sensor equipment, efficiency of cooling system, impedance, vacuum, etc. In addition to the SPS test, also a robustness experiment was carried out at the TT40 extraction line. Amongst others, the following tests were carried out at the SPS:

- Mechanical functionalities and main control;
- Beam based centring and alignment;
- Halo dynamics and beam shaping with jaws;
- Heating of collimator and cooling water;
- Systematics of BLM system;
- Impedance and trapped modes;
- Tune versus collimator opening;
- Vacuum/out gassing (e-cloud).

Table 3: Parameters of the low and high intensity beams set up at the SPS for the collimator test.

Parameter	Low Int.	High Int.
Energy [GeV]	270	270
Bunch population [10^{11}p]	≈ 1.1	≈ 1.1
Number of bunches	$1 - 16$	$72 - 288$
Beam intensity [10^{12}p]	$0.1 - 1.8$	$7.9 - 32$
Norm. emittance [μm]	≈ 1.0	≈ 3.75
Horiz. beam size [mm]	≈ 0.4	≈ 0.7

This section does not provide an exhaustive summary of all performed measurements but rather a selection of some examples that are relevant for the commissioning of the collimators at the LHC.

It is noted that a dedicated set of beam loss monitors (BLM's) was installed for the collimator test. Eight BLM's were mounted around the vacuum chamber, a few meters downstream of the collimator (two sets of four BLM's, located at 9 and 12 metres from the collimator). The BLM system was mainly used as a tool to align the collimator jaws with respect to the beam. In addition, dedicated measurement of BLM systematics were also carried out [13]. An on-line reading on the BLM's at the control room was used for the beam based alignment of the collimator and data were also recorded for detailed off-line analyses.

Beam-based alignment of the collimator jaws

The procedure for centring the collimator jaws with respect to the beam centre is illustrated in Fig. 15. A jaw, say the right one, is moved towards the beam and left at a given distance from its centre. Due to the betatron motion of the beam particles, both beam sides are scraped and this provides a "sharp" reference edge for the other jaw, which is then moved towards the beam in small steps. Ideally, the downstream BLM's should measure some proton losses only when the left jaw reaches the same distance from the beam centre as the right jaw. This procedure would then provide a centring of the jaw with a precision fixed by the step size. In addition, by moving one jaw corner per time,
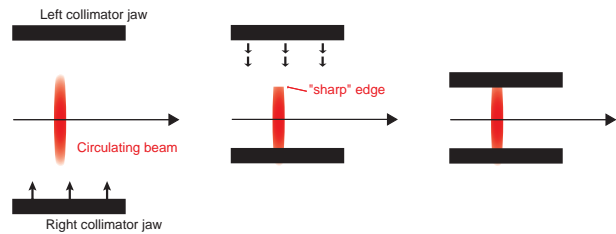

Figure 15: Procedure to centre the collimator jaws around the circulating beam: the beam is scraped with one jaw and the other jaw is moved towards the beam until beam losses are measured by the BLM's.
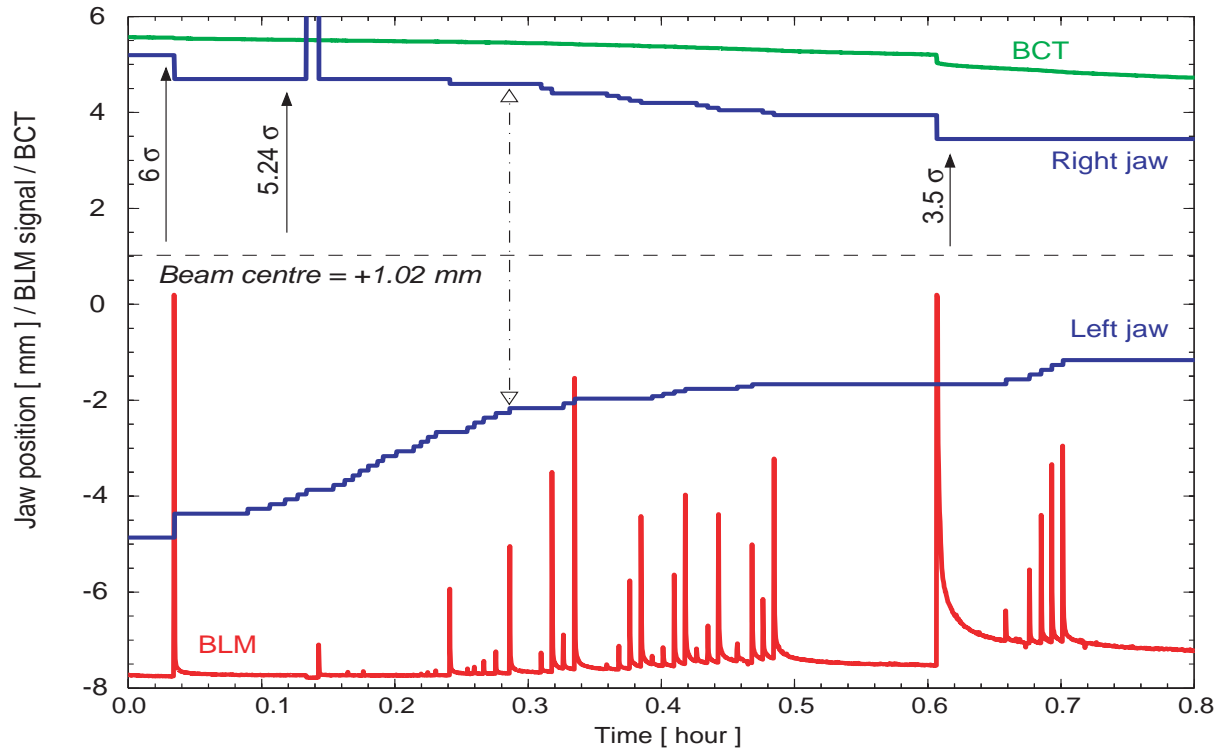
Figure 16: Example of a jaw centring carried out at the SPS by following the procedure of Fig. ref. In the bottom graph, given are the jaw positions in millimetres with respect to the collimator centre (blue lines), the BLM signal (red lines, arbitrary units) and the beam intensity as measured with a BCT (green line, arbitrary units), versus time.

one could also use this method to adjust the jaw angle with respect to the beam envelope.

Figure 16 shows how the alignment procedure was actually carried out at the SPS. Data refer to the first collimator centring performed with the highest intensity beam (4 LHC -like batches of 72 bunches with 25 ns spacing, for a total intensity of 3×10^{13} protons). Based on emittance measurements, the expected beam size was approximately 0.7 mm. Shown are the jaw positions with respect to the collimator centre (blue lines), the BLM signal (red line) and the beam intensity (BCT, green line). The right jaw was moved to a depth of approximately 5.2 σ to scrape the beam (first large peak in the BLM reading) and then the left jaw was moved in steps of 100 μm until a significant losses were measured (spike at approximately 0.3 h). Then, a finer centring in steps of 50 μm was also performed. Three or four consecutive displacements of right and left jaw produced similar series of loss peaks, as expected if the two jaws were at the same distance from the beam centre. We concluded that the collimator centring to the 50 μm level was achieved. Scraping the beam down to the 3.5 σ level induced losses of few percent of the total beam intensity, which is consistent with the expected beam population.

It is noted that (1) the knowledge of the beam size relied on emittance measurements performed with wire scans [14] and on the MAD calculation of the beta functions at the collimator. (2) The total alignment procedure took slightly more than 0.5 h in the considered example. Par-

ticular care was taken in this case because this was the very first test with high intensity beam. Other alignments, routinely carried out when needed (e.g., every time a new beam with different parameters was filled in the machine) typically took between 10 and 20 minutes. (3) The alignment procedure relies on a good orbit stability, that was achieved in most of the cases at the SPS.

As a cross-check of the beam-based alignment, we tried to find the beam centre by completely scraping the beam with one jaw. In this case, the beam current should drop to zero when no beam is left, i.e. when the jaw reaches the beam centre. This is illustrated in Fig. 17. By comparing the jaw position (top graph) with the BCT signal (bottom graph), it is found that the estimated beam centre agrees to within better than one sigma (i.e., to the $\approx 500\,\mu$m level) with the BLM based beam centring that was performed approximately 2.5 hours before. Various tests were carried out between the two alignment procedures and it not excluded that orbit drifts may have occurred. Another procedure for the beam alignment with the BCT measurement was successfully tested with the collimator installed at the transfer line [12].

Measuring the beam size by scraping the beam with the collimator

The bottom plot in Fig. 17 suggests than one could infer the beam size from the profile of the beam current while the
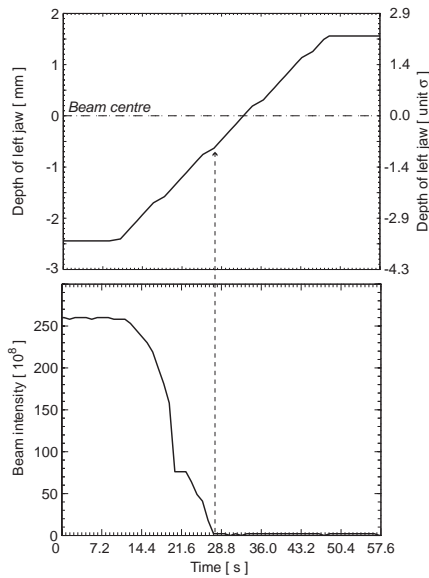
Figure 17: Jaw position (top) and beam current (bottom) as a function of time while the beam is being scraped with one collimator jaw.

beam is being scraped with the collimator. By assuming a Gaussian transverse beam distribution and by neglecting dispersion and coupling (which were in any case negligible at the collimator location), one can show that the relative beam population, $F(x)$, is given by [15, 16]

$$F(x) = 1 - \exp\left(\frac{-(x - x_0)^2}{2\sigma^2}\right), \qquad (10)$$

where x denotes the jaw position, x_0 is the beam centre and σ is the transverse beam size. This formula is derived by assuming that the jaw motion is slow with respect to the betatron frequency and hence one jaw is sufficient to radially scrape the beam in phase-space [16]. Figure 18 shows two examples of beam scrape measurements performed at the SPS. The measured values of the function $F(x)$ (crosses) and its Gaussian fit (red lines) are given. The measured data agree with the theoretical expectations for Gaussian beams. The beam sizes calculated from the Gaussian fit
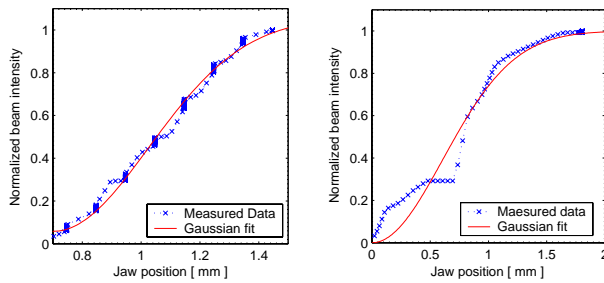

Figure 18: Beam current versus collimator depth while the beam is being scraped with one jaw. Measured data (crosses) and Gaussian fit (line) are given of a low (left) and a high intensity (right) case. The fitted beam sizes are $325 \pm 3\,\mu$m and $625 \pm 52\,\mu$m, respectively.
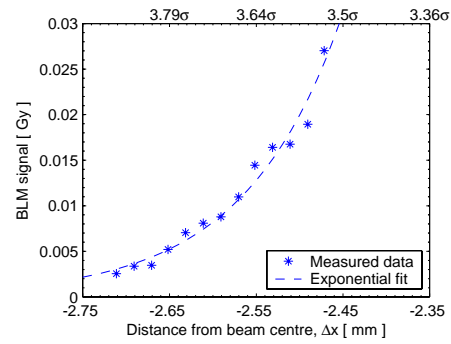

Figure 19: BLM signal versus jaw depth obtained when scraping the beam tail with. One jaw is set to increasing depth values. Before each step, the jaw is retracted and kept at a distance of $\approx 25\,\sigma$ from the beam centre for a fixed time to reproduce the same tail population.

are $325 \pm 3\,\mu$m for the low intensity beam (left graph) and $665 \pm 52\,\mu$m for the high intensity beam (right graph), which is in good agreement with the sizes estimated from the emittance measurements. This method could in principle be used in the commissioning of the LHC collimation system to measure the local beam size and to adjust the collimator gap but has the disadvantage that it can only be performed with low beam intensities. The extrapolation of the calculated beam sizes to higher intensity beams remains to be assessed.

Scan of tail population

The SPS experience shows that the alignment procedure described in the previous section is limited by the fact that the "sharp" beam edge produced by scraping the beam with one jaw shows exponential tail. An example is shown in Fig. 19 for a high intensity beam. Similar profiles where measured with beams of different intensities as with different collimator depths. Our present understanding is that, if the two jaws are within the exponential, centring the jaw within better than $50\,\mu$m becomes challenging. On the other hand, a proper knowledge of the beam tail population could be used to infer the jaw depth from the BLM signal directly. This procedure would require detailed understanding of tail population and halo particle dynamics

Adjusting the collimator angle

In order to measure the jaw angle with respect to the beam envelope, one jaw was moved from an "out" position at $\approx 15\,\sigma$ from the beam centre to an "in" position at $4\,\sigma$. The procedure was repeated for three different jaw angles. In Figure 20 the average value of the measured BLM signal in the various cases is plotted as a function of the jaw angle. In order to reproduce the same tail population for the various jaw orientations, the beam tail was scraped for a fixed time with a reference angle before each new scraping. In principle, the obtained BLM signal could be used to infer the relative angle between beam envelope and col-
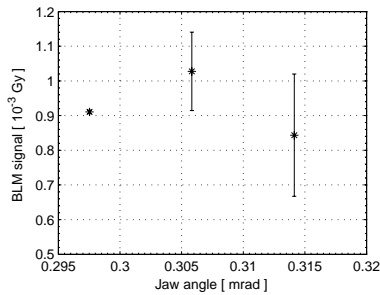
Figure 20: Average value of the BLM signals as measured when scraping the beam at $4\,\sigma$ with different jaw angles.

limator jaws as a function of the collimator settings. This would allow adjusting the collimator angle with respect to the beam envelope. The available statistics for the SPS data is poor and additional measurements are be required to better understand the systematics of this procedure.

CONCLUSIONS

The design LHC aperture is $7.5\,\sigma$ at injection and $8.1\,\sigma$ at top energy (squeezed optics with $\beta^* = 0.55\,\mathrm{m}$). This is below the design goal of $8.5\,\sigma$. A local loss of 0.5 sigma could result in a factor 6 higher losses at some cold magnets. There is practically no operational margin to optimize the aperture during commissioning because, by design, all the margins for beta-beat and closed orbit errors were taken into account with no contingency.

The developed tools enhance considerably the state-of-the-art simulations of beam loss for hadron machines and proved to be a valuable tool to better understand the performance of the collimation system and the loss patterns. It is now possible to precisely estimate the azimuthal and transverse distribution of losses at the various LHC elements. This should be used as an input for future studies of proton induced quenches. In addition, the loss maps can also be used as an input for the BLM system response study and hence can help in the commissioning of the BLM system.

Loss patterns around the ring show loss spikes above the assumed quench limits even for a perfect machine. Machine imperfection such as closed orbit errors can induce losses 10 times larger than the quench limit at various locations. Some locations will be protected by additional absorbers, which are presently being finalized and have not been included yet in the model. Nevertheless, several locations will not be protected by the absorbers. Additional imperfections of the cleaning insertion (e.g., jaw alignment and centring) or optics errors (e.g., coupling, higher order field errors), not yet taken into account, are expected to further increase losses.

The collimator tests with beam at the SPS were also reviewed. The beam based collimator alignment carried out with the BLM system suggests that a jaw centring to the $\approx 50\,\mu\mathrm{m}$ can be achieved. This procedure was only cross-checked with a destructive measure of the beam centre based on a beam scraping, carried out 2.5 hours after the

BLM based alignment. The two procedures agree within $\approx 500\,\mu\mathrm{m}$ but orbit drift might have occurred between the two measurements. The typical required time for the BLM alignment is ≈ 15 minutes per collimator. Some ideas were proposed to adjust the collimator depth the the local beam size. Angle adjustment was difficult but in principle can be done. Better understanding of particle dynamics and testing of faster and more accurate algorithms for collimator settings would certainly profit from additional beam time at the SPS in 2006.

ACKNOWLEDGEMENTS

REFERENCES

[1] J.B. Jeanneret, D. Leroy, L. Oberli and T. Trenckler, "Quanch levels and transient beam losses in the LHC magnets," CERN-LHC-PROJECT-REPORT-44 (1996).

[2] R. Aßmann, "Collimators and cleaning: could this limit the LHC performance?," LHC Performance Workshop, Chamonix XII, Chamonix, FR (2003).

[3] J.B. Jeanneret and R. Ostojic, "Geometrical acceptance in LHC version 5.0," CERN-LHC-PROJECT-NOTE-111 (1997).

[4] R. W. Assmann et al., "Expected performance and beam-based optimization of the LHC collimation system," EPAC2004, also as CERN-LHC-PROJECT-REPORT-758 (2004).

[5] J. B. Jeanneret, "Optics of a two-stage collimation system," Phys. Rev. ST Accel. Beams **1** (1998) 081001.

[6] http://mad.home.cern.ch/mad/

[7] T. Trenkler and J.B. Jeanneret, CERN SL/Note 94-105 (AP), 1994.

[8] F. Schimdt, CERN SL/94-56 (AP), 1994.

[9] R. Assmann, F. Schmidt, F. Zimmermann and M. P. Zorzano, "Equilibrium beam distribution and halo in the LHC," EPAC2002, also as CERN-LHC-PROJECT-REPORT-592 (2002).

[10] R. Aßmann, these proceedings.

[11] A. Siemko and M. Calvi, these proceedings.

[12] V. Kain et al, these proceedings.

[13] B.E. Holzer, these proceedings.

[14] Federico Roncarolo, CERN-AB-ABP, private communication (October 2004).

[15] A. Jansson, "Collimator scans to measure Tevatron emittance," Tevatron beam study report (2003).

[16] H. Burkhardt and R. Schimdt, "Intensity and luminosity after beam scraping," CERN-AB-2004-032 (2004).